



Full Length Article

Intrinsic sodium occurrence in Zhundong coal: Experimental observations and molecular modeling

Cen Sun^{a,b}, Xiaolin Wei^{a,b}, Running Kang^{a,b}, Feng Bin^{a,b}, Sen Li^a

^a State Key Laboratory of High-Temperature Gas Kinetics, Institute of Mechanics, Chinese Academy of Sciences, Beijing 100190, China

^b School of Engineering Science, University of Chinese Academy of Sciences, Beijing 100049, China



ARTICLE INFO

Keywords:

Alkali metal occurrence model
Zhundong coal
Molecular model
DFT
NMR

ABSTRACT

Detailed intrinsic sodium occurrence for future research on migration, release, and catalyst effect behavior of sodium is necessary. Complementary characterizations, such as ^{13}C CP/MAS NMR, FT-IR, ^{23}Na CP/MAS NMR, XPS, elemental composition analysis, and sequential extraction experiments, were employed to elucidate the actual compound form of sodium as well as Zhundong coal's structural features. Thus, a molecular occurrence model of sodium in Zhundong coal was constructed based on its structural characteristics via computational chemistry. The occurrence model of alkali metals in Zhundong coal, including their compound form, relative content, and distribution properties, was investigated at the microstructural level. Preliminary results show that the amorphous cell formula of Zhundong coal is $(\text{C}_{2080}\text{H}_{980}\text{O}_{380}\text{N}_{30}\text{S}_{10}\text{Na})_n$. Organic oxygen in Zhundong coal was 67.7% hydroxyl (ethoxy), 15.5% carbonyl, and the remaining 16.8% was attributed to carboxyl. Combined with the ^{23}Na CP/MAS NMR and sequential extraction experiment, organic sodium accounts for 18.01% of the total. Most inorganic sodium (81.99%) is present as hydrated sodium ion (75.08%), while a small part is present as NaCl crystal phase (3.34%) insoluble-sodium account for 3.57%. Calculated ^{13}C NMR, FT-IR, and ^{23}Na NMR spectra of the proposed model agree well with the experimental spectra suggesting that the molecular occurrence model of sodium in Zhundong coal is a particularly convincing model at the approximate condition of statistical average. The highest negative electrostatic potential area is near the carboxyl group and may be attributed to organic sodium absorption sites; the hydroxy or phenoxy group nearby may form additional coordination bonds to sodium, indicating the reflection of the complexity of the Na chemical environment as concluded from ^{23}Na CP/MAS NMR.

1. Introduction

Although increasing attention has been paid to renewable energy, coal still accounted for 27% of the world's primary energy consumption in 2019 [1]. With proven reserves of over 390 billion tons, the newly discovered Zhundong coalfield (Eastern Part of Zhunge'er, Xinjiang province, Northwest China) is anticipated to cover China's energy needs for future decades [2]. However, the content of alkali metals in this coal (0.2%–0.7%) is much higher than in conventional power coal [3,4]. As intrinsic components, alkali metals can influence mineral migration during the combustion and pyrolysis, thus causing equipment safety problems such as ash slagging, fouling, corrosion of heat transfer

surfaces in furnaces, or high-temperature corrosion of gas turbine blades in integrated gasification combined cycling [5,6]. To solve these problems, understanding the characteristics of these alkali metals is essential. To address the negative impact of Zhundong coal's high sodium characteristics and formulate a method for its safe and efficient utilization, we must first clarify the occurrence characteristics of alkali metals in the coal. And then to investigate the release characteristics of Zhundong coal to realize the micro-regulation of alkali metal migration behavior in Zhundong coal combustion.

Substantial research on the occurrence of alkali metals in Zhundong coal has been carried out in recent years [7]. Most of the AAEM (alkali and alkaline earth metals) in Zhundong coal consists of sodium. Bai

Abbreviations: AAEM, alkali and alkaline earth metal; CP/MAS NMR, cross-polarization magic angle spinning nuclear magnetic resonance; DFT, Density functional theory; ESP, Electrostatic Potential; FT-IR, Fourier transform infrared spectroscopy; GCMC, Grand canonical Monte Carlo; MD, Molecule Dynamics; MM, molecular mechanics; Reaxff-MD, Reactive force field molecular dynamics; NVT ensemble, Canonical ensemble; NPT ensemble, Isothermal-isobaric ensemble; NVE ensemble, Micro-canonical ensemble; XPS, X-ray photoelectron spectrometry.

E-mail address: xlwei@imech.ac.cn (X. Wei).

<https://doi.org/10.1016/j.fuel.2021.121491>

Received 3 April 2021; Received in revised form 14 July 2021; Accepted 17 July 2021

Available online 28 July 2021

0016-2361/© 2021 Elsevier Ltd. All rights reserved.

Table 1
Proximate, ultimate analysis, and ash analyses of Zhundong coal.

Proximate analysis $w_{ad}/\%$				Ultimate analysis $w_{ad}/\%$									
M_{ad}	A_{ad}	V_{ad}	FC_{ad}	C	H	O	N	S					
11.36	6.70	27.31	54.63	62.57	2.46	15.08	1.03	0.80					
Ash analyses of Zhundong coal/ $\%$													
SiO_2	Al_2O_3	Fe_2O_3	CaO	MgO	SrO	TiO_2	Cl	SO_3	MnO	P_2O_5	ZnO	K_2O	Na_2O
11.00	8.14	11.84	31.95	5.42	0.14	0.51	4.68	18.17	0.20	0.37	1.61	0.54	5.42

Note: ad = air-dry basis

(2015) studied the content distribution of sodium in different size fractions, density, and maceral groups and found that water-soluble sodium is the dominant form of sodium in Zhundong coal; the sodium content reaches up to 2–10 wt% [8]. Sequential extraction experiments [9] have also been widely used to identify different forms (water-soluble, exchangeable, acid-soluble, and insoluble) of AAEM in solid fuel [10,11]. Based on the sequential extraction method, scholars discussed the content of sodium in Zhundong coal in different locations, densities [12], and depth to the coal seam roof [3]. Water-soluble sodium and ammonium acetate-soluble sodium generally exceed 80%. The sequential extraction method used in these publications is an indirect method to evaluate the content of different soluble alkali metals in coal by measuring the alkali metals in the extraction solution of the coal. However, this method does not clarify the actual compound form of sodium present in the original coal. In the water-soluble sodium in Zhundong coal, the proportion of hydrated ions and NaCl crystal phases is unclear and is not clarified by the sequential method used in the papers above. At the same time, it is unclear how the organic sodium is combined with the coal matrix and how the strong polarity of alkali metals affects the coal matrix. Understanding the occurrence of alkali metals in Zhundong coal by categorizing sodium elements according to solubility is insufficient. These issues restrict the development of precise reaction mechanisms for alkali metals in the thermochemical conversion process.

Quantum chemical calculations allow the understanding between microstructures and macroscopic experimental observations. Some studies on the occurrence, migration, and transformation of C, N, and S in solid fuel use molecular modeling and computational chemistry [13,14]. Few accurate molecular occurrence models for alkali metals have been reported [15–20]. A carbonaceous mode with calcium atom chemisorption directly to a single-layer graphene structure containing pyridine was chosen as a calcium occurrence molecular model by Chen et al. (2020) to study the formation mechanism of NH_3 and HCN during pyrolysis in the presence of calcium [21]. Here, a direct connection between the calcium and carbon matrix is far different from the experimental observation, and the single-layer graphene structure is far from the three-dimensional reticular structure of Zhundong coal. Hong et al. (2019) [22] added calcium in the form of (-COO-Ca-OOC-) of calcium carboxylate into the coal molecular model and constructed an occurrence model of organic calcium. The model did not refer to the electrostatic potential distribution to determine the specific adsorption position of calcium in coal. It also did not adjust and verify via spectral experiments.

Structure and function are closely related, and the microstructures of alkali metal occurrence have an important influence on the release process and catalysis of alkali metals. Macromolecular models are essential for investigating the structure–activity relationship in the thermochemical conversion process (sodium emission mechanism) as well as slagging, fouling, and corrosion mechanisms during the thermal conversion processes. Molecular reconstruction of the occurrence model of alkali metals can provide data and structural model support for subsequent studies of the catalysis, combustion, and coking of alkali metals using reactive force field molecular dynamics (Reaxff-MD) and quantum chemistry.

Table 2
Analysis of sodium in Zhundong coal.

Sample	Water-soluble	Exchangeable	Acid-soluble	Insoluble	Sodium content
Zhundong coal	78.42 wt %	11.57 wt %	6.44 wt %	3.57 wt %	0.322 wt %

The molecular model of sodium metals is closely related to the molecular structure of Zhundong coal. It is difficult to discuss the occurrence characteristics of alkali metals in coal without the molecular structure of Zhundong coal; thus, experimental observation and model study on the molecular structure of Zhundong coal play an essential role in the investigation of the occurrence characteristics of alkali metals, including their compound form, relative content, and distribution properties.

Therefore, in this work, we primarily concentrate on occurrence characters of sodium in Zhundong coal and present a reasonably realistic alkali metal occurrence model via comprehensive experiments and computational chemistry (^{23}Na -CP/MAS NMR and sequential extraction experiments serve for sodium occurrence; FT-IR, XPS, ^{13}C -CP/MAS NMR, and proximate and ultimate analysis serve for Zhundong coal structure). This work is expected to clarify the actual microstructure characteristics of sodium in Zhundong coal and provide a practical approach for building AAEM occurrence models in the quantification and visualization in high-alkali coal, which is helpful for the future development of alkali metal reaction and release characteristics.

2. Methodologies

2.1. Material

Raw coal from the Zhundong coalfield Wucaiwan coal mine was crushed on a coal mill and sieved by an oscillator. The pulverized coal had a particle size of 88–125 μm and was selected as the sample in this work. Proximate, ultimate analyses are illustrated in Table 1 and were conducted following the China National Standards (GB/T212-2008, GB/T214-2007, GB/T476-2008, and GB/T19227-2008) at China National Coal Quality Supervision and Testing Center. The chemical composition of coal ash was obtained using an X-ray fluorescence spectrometer (ARLAdvant'X IntellipowerTM 3600), as detailed in Table 1.

2.2. Sequential extraction

Sequential extraction experiments were performed to obtain different forms (water-soluble, exchangeable, acid-soluble, and insoluble) of sodium in coal. Deionized water, ammonium acetate ($1.0 \text{ mol}\cdot\text{L}^{-1} \text{ CH}_3\text{COONH}_4$), and hydrochloric acid ($1.0 \text{ mol}\cdot\text{L}^{-1} \text{ HCl}$) were used to extract coal samples sequentially for 24 h at 60 °C. The solid to liquid ratio was 1 g to 50 ml. The alkali metals' content was determined by inductively coupled plasma-optical emission spectroscopy (ICP-OES), as shown in Table 2. More information is available in our previous work [23].

2.3. ^{13}C and ^{23}Na CP/MAS NMR experiments

In this work, ^{13}C and ^{23}Na cross-polarization magic angle spinning nuclear magnetic resonance (CP/MAS NMR) experiments were used to provide the carbon skeleton and occurrence of Na, respectively. The carbon structure parameters of Zhundong coal offer essential information on the composition of aromatic condensation rings in the macromolecular model of Zhundong coal.

The ^{13}C CP/MAS NMR test for Zhundong coal was conducted using a Bruker NEO 400 M Model nuclear magnetic resonance instrument with a ^{13}C testing frequency of 10 kHz, the acquisition time of 35.0 ms, recycle delay time of 2.0 s, and contact time of 0.2 ms.

An Agilent 600 DD2 spectrometer was used to perform ^{23}Na CP/MAS NMR tests with a resonance frequency of 158.65 MHz and a recycle delay time of 5.0 s. The spectra were recorded at room temperature with an 8 kHz frequency and a 4 mm probe.

2.4. FT-IR analysis

The organic functional group of coal samples was detected by Fourier-transform infrared spectroscopy (FT-IR) experiments using a Nicolet NETXUS670 spectrometer with a KBr tablet (the mass ratio of the coal sample to KBr was 1:250); the spectral range was between 400 and 1800 cm^{-1} . Spectra were sequentially recorded with a resolution of 4 cm^{-1} and with an accumulation of 30 scans.

To obtain quantitative information, the Gaussian peak shape function was selected to fit the FT-IR spectra. The characteristic absorption peaks of the infrared spectra of coal samples are distributed in two regions [24]: oxygen-containing functional groups ($1800\text{--}1000\text{ cm}^{-1}$) and aromatic functional groups in the $900\text{--}700\text{ cm}^{-1}$.

2.5. XPS analysis

X-ray photoelectron spectroscopy (XPS) experiments determined nitrogen and sulfur occurrence from coal samples. XPS experiments used a Thermo Fisher Esca Lab 250Xi spectrometer at an emission angle of 0.1° with a filament energy source of 14.7 keV and a filament current of 10 mA using a monochromatic Al K α source. A charge neutralizer was used to balance the charge of the sample. Measurements were carried out in the 0.5 mm^2 area and 30 eV pass energy range. The samples were corrected by the standard binding energy of adventitious carbon (C 1s) to 284.8 eV. To obtain quantitative information, the Gaussian peak shape function was selected to fit the XPS Spectra.

2.6. Construction method of coal matrix structure

Hong et al. (2019) constructed a macromolecular model of Zhundong coal for the first time [22] by revising the hatcher bituminous coal model [25]. However, they did not utilize spectral information such as NMR (nuclear magnetic resonance) or FT-IR (Fourier transformed infrared) spectroscopy to adjust and verify the macromolecular structure. Meanwhile, N, S, Na, and other heteroatoms are not involved in the constructed coal model.

Quantum chemical calculations allow connections between structure and spectra to be understood at the microstructural level. Therefore, spectroscopic experiments can be used to infer the molecular structure through quantum chemical calculations. Synthesizing the structural parameters obtained from the abovementioned experiments (FT-IR, XPS, and ^{13}C -CP/MAS NMR, as well as proximate and ultimate analyses for Zhundong coal) and with reference to the widely accepted Wisser's bituminous coal model [26] and Shinn's bituminous coal model [27]. An initial guessed structure was proposed (ether bridge, lipid bridge/ring was chosen as the primary connection between aromatic condensation rings and side chain, functional group). To verify the fidelity of the proposed molecule structures, a comparison was conducted between the experimental ^{13}C NMR, FT-IR spectrum of Zhundong coal and that

calculated by B3LYP/6-31 basis set and MestRevona. The bridging and functional groups' positions were adjusted to keep the macromolecular model's aromaticity unchanged during the adjustment process until the calculated FT-IR ^{13}C NMR spectrum could reproduce the experimental data.

The molecular interactions between the repetitive units are essential for forming the three-dimensional reticular coal structure. The amorphous cell model of Zhundong coal was constructed using the molecular configuration of Zhundong coal constructed via molecular dynamic (MD) simulations using an amorphous cell module in the Material Studio platform. According to elemental and sequential extraction experimental data, the proposed molecular configurations of the Zhundong coal were, as the basic unit, placed in a periodic box at a particular proportion. The amorphous cell model's initial density was set to 0.1 g/m^3 to avoid overlapping functional structures. To make the density reasonable, a series of molecular dynamic optimizations were performed on the initial amorphous cell model. The Dreiding force field was used for geometric optimization, and annealing calculations were done on the molecular structure according to reported work [28]. Annealing dynamic simulations were performed with an annealing cycle from 300 to 800 K in the NVT ensemble. Compression and decompression MD simulations were done at pressures of 20 MPa and 0.02 MPa within the NPT ensemble, respectively. The last part is a dynamic simulation using an NVE ensemble. This ended with a stable and low-energy structure. The simulated temperature ranged from 300 to 800 K (temperature step 10 K), and the single component pressures ranged from 0.02 to 20 MPa. This covers the Zhundong coal seam, including its geothermal and stratigraphic pressures. The simulated temperatures ranged from 300 to 800 K, and the single component pressures ranged from 0.02 to 20 MPa, thus could cover the reservoir pressure and temperature of the Wucaiwang coal mine in Zhundong coalfield [29].

2.7. Alkali metal microstructure reconstruction method

The cause of high sodium in Zhundong coal is infiltration of high salinity (NaCl , Na_2SO_4) groundwater into the coal seam [8]. Coal acts as an ion-exchangeable medium [30]. Adsorption and cation exchange during coal formation are essential factors influencing the alkali metal occurrence. We cannot add sodium to the coal molecular model using traditional modeling methods. Given the high sodium characteristics of Zhundong coal, we have made some developments in traditional coal molecular modeling methods for alkali metal microstructure reconstruction, specifically as follows:

The electrostatic potential of the Zhundong macromolecular model was analyzed by the wavefunction software Multiwfn to identify the coordination position of Na ions (organic sodium) on the matrix of Zhundong coal [31]. The surface electrostatic potential map was visualized using VMD [32]. The negative electrostatic potential makes this region susceptible to adsorption of H^+ , Na^+ , K^+ , and other cations at the late stage of coal formation. The more negative electrostatic potential is seen, making it easier for cations to be drawn in. Therefore, the highest negative electrostatic potential area was chosen as the sodium adsorption site.

In search of inorganic sodium (water-soluble), the adsorption position between basic units in the amorphous cell of Zhundong coal, molecular dynamics, and grand canonical Monte Carlo (MD-GCMC) simulations were conducted using material studio software to obtain an amorphous cell with water and NaCl absorbed.

2.8. Calculation detail

Density functional theory (DFT) is too expensive to apply to the macromolecular configuration directly. A relatively stable geometric configuration is imperative for DFT simulation, obtained by geometric optimization and annealing calculation using molecular mechanics (MM) and molecular dynamics (MD) theory. MM and MD simulations

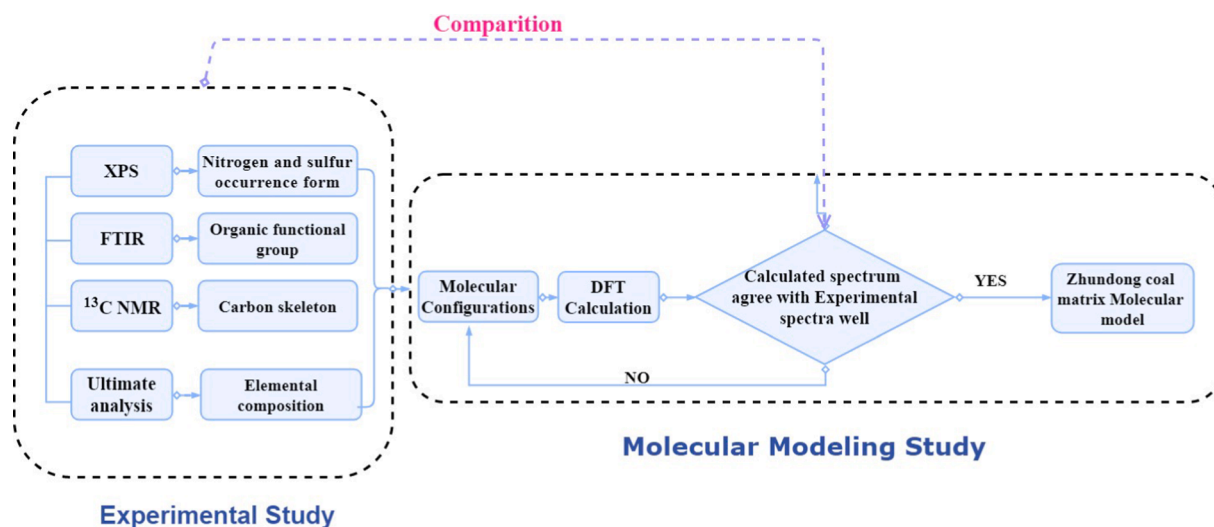


Fig. 1. The construction method of a coal matrix structure.

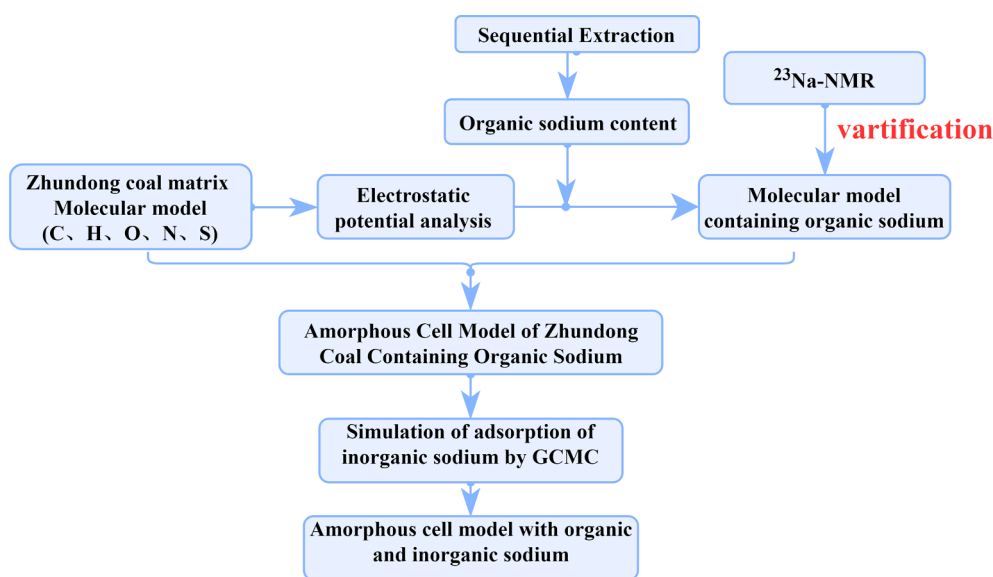


Fig. 2. Alkali metal microstructure reconstruction method.

were conducted on the Material Studio platform. The Dreiding force field was used to calculate the molecular structure's geometric optimization and annealing calculation [28]. Annealing initial temperature was set at 300 K, and the maximum temperature was controlled at 800 K. Thermostat was Nose, and the number of cycles was 50. The time step

is 0.001 ps, and the simulation time is 10 ps.

The B3LYP [33,34] method is more effective than M062X [35] method in describing molecular vibrations; it has a better convergence property than M062X in the case of a large system size (>250 atoms). Therefore, the optimization, nuclear magic resonance, and frequency simulation were performed using the B3LYP method and the 6-31 base group. All quantum chemical calculations were performed using Gaussian 09 software.

3. Results and discussion

3.1. Identification of the elemental composition

The elemental composition was the most critical parameter for coal model construction. Water-soluble sodium mainly exists in crystals or hydrated ions sodium [23]. The organic sodium content in Zhundong coal is shallow—only 0.048% (convert to dry and ash-free base). The molecular formula of Zhundong coal macromolecules contains a single sodium atom and is $(C_{2080}H_{980}O_{380}N_{30}S_{10}Na)_n$.

Coal is a polymer-like substance. It is composed of several basic units

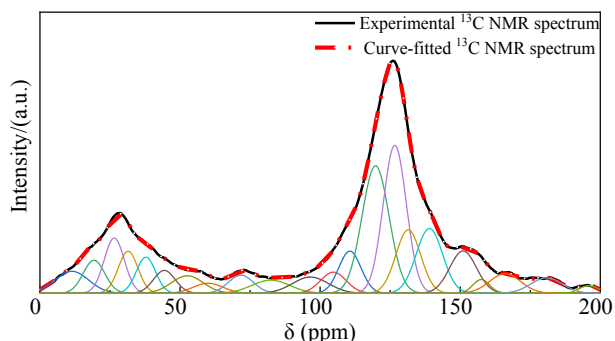
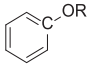
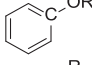
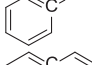
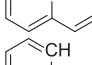
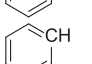
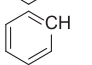
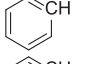
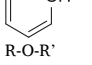
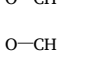


Fig. 3. ^{13}C NMR (CP/MAS) spectra of Zhundong coal sample.

Table 3
Curve-fitted ^{13}C -NMR(CP-MAS) for Zhundong coal.

Chemical shift δ , ppm	Assignment		Molar content/%
195.87	—CHO	ketones, C=O in aldehydes, and quinones	0.68%
180.81	—COOH	COOR groups and C=O in COOH	2.29%
166.03	—COOH	—COOR groups and C=O in COOH	2.88%
157.51		O-substituted aromatic C in phenols and Aromatic ethers	1.08%
151.03		O-substituted aromatic C in phenols and aromatic ethers	5.34%
139.01		Alkyl substituted aromatic carbon	8.06%
131.46		Bridgehead aromatic carbon	7.42%
126.66		Protonated aromatic carbon	16.16%
119.78		Protonated aromatic carbon	16.26%
110.62		Protonated aromatic carbon	4.43%
104.73		Protonated aromatic carbon	2.55%
96.56		Protonated aromatic carbon	2.75%
82.38	R—O—R'	O-bonded C in carbon hydrates	2.34%
71.73	O—CH	Alcohols and O substituted aliphatic C in ethers	2.14%
60.03	O—CH	Alcohols and O substituted aliphatic C in ethers	1.41%
52.61	O—CH ₃ , O—CH ₂	Methoxy C	2.63%
44.40	—CH—C	Quaternary C; methylene or methine C alpha to the aromatic ring	2.34%
37.82	—CH ₂	Cyclic or acyclic methylene C	3.27%
31.47	—CH ₂ —C	Quaternary C; methylene or methine C alpha to the aromatic ring	3.89%
26.52	—CH ₂	Cyclic or acyclic methylene C	5.24%
19.28	Ar—CH ₃	Methyl C on an aromatic ring	3.36%
11.41	R—CH ₃	Terminal methyl	3.47%

of similar structure. If the smallest unit contains one sodium atom, then this single molecule is $(\text{C}_{2080}\text{H}_{980}\text{O}_{380}\text{N}_{30}\text{S}_{10}\text{Na})_n$, which is too large for quantum chemical calculations. Therefore, sulfur was chosen as the reference. We split the coal molecule $(\text{C}_{2080}\text{H}_{980}\text{O}_{380}\text{N}_{30}\text{S}_{10}\text{Na})_n$ into small molecules with and without sodium ($\text{C}_{208}\text{H}_{98}\text{O}_{38}\text{N}_3\text{S}_1$ and $\text{C}_{208}\text{H}_{98}\text{O}_{38}\text{N}_3\text{S}_1\text{Na}$, respectively). To ensure that the total content of sodium elements in the model is consistent with the experiment, molecules without and with sodium atoms are placed into periodic boxes in proportion to their elemental composition, and the molecule of Zhundong coal amorphous cell can be expressed as $(\text{C}_{208}\text{H}_{98}\text{O}_{38}\text{N}_3\text{S}_1)_9 \cdot (\text{C}_{208}\text{H}_{98}\text{O}_{38}\text{N}_3\text{S}_1\text{Na})$. (See Fig. 1, Fig. 2)

Table 4
Carbon structural parameters of the Zhundong coal.

f_{al}	f_{al}^O	f_{al}^c	f_{al}^H	f_a	f_a^c	f_a^H	f_a^c	f_a^P	f_a^N	f_a^B	f_a^S
30.09%	8.52%	6.83%	14.74%	69.91%	64.05%	42.15%	5.85%	6.42%	21.90%	7.42%	8.06%

f_{al} —aliphatic, f_{al}^O —bonded to oxygen, f_{al}^c —CH₃ or unprotonated, f_{al}^H —CH— or CH₂, f_a —aromatic, f_a^c —alkylated aromatic, f_a^H —aromatic and protonated, f_a^c —carbonyl, f_a^P —phenolic or phenolic ether, f_a^N —unprotonated and aromatic, f_a^B —in an aromatic ring, f_a^S —aromatic bridgehead

3.2. Identification of carbon skeleton structure

The ^{13}C CP/MAS NMR spectrum in Fig. 3 shows that carbon structure parameters can be determined by Gaussian fitting, as revealed in Table 3. A higher condensation degree of the aromatic ring leads to a larger value for the X_{BP} (the ratio of bridge carbon to peri carbon number X_{BP}) parameter. Table 4 shows that the X_{BP} of Zhundong coal is 0.13. X_{BP} parameters for benzene, naphthalene, and anthracene were 0, 0.25, 0.4, respectively. Anthracene and aromatic rings with a higher degree of condensation are rare in low-rank coals; benzene rings followed by naphthalene consist of the aromatic rings in Zhundong coal. X_{BP} is calculated using the following equation:

$$X_{BP} = f_a^B / (f_a^H + f_a^P + f_a^S) \quad (1)$$

3.3. Identification of existing sodium forms

The ^{23}Na CP/MAS NMR spectrum in Fig. 4 shows broad asymmetric lines extending from 15 ppm down to values beyond -37 ppm. Broad and resonance lines with shapes similar to the biomass have been reported [36]. The peak at the center of 7 ppm mainly corresponds to the NaCl crystal. The peak area at this point is relatively small and indicates that NaCl occupies a relatively small proportion of the total sodium species. The sequential extraction experiment indicates that organic sodium accounts for 18.01%. And most inorganic sodium (81.99%) is found to present as hydrated ion sodium (75.08%), while a small part as NaCl crystal phase (3.34%), which demonstrated that most of the water-soluble sodium is present as hydrated ion sodium; a small part is NaCl crystals.

The peaks at the center of -28 to -1 ppm are mainly associated with sodium in “—ONa”, “—COONa”. The disordered local environment involving Na-O distances and the coordination number of the sodium have different shifting effects on the chemical displacement of ^{23}Na NMR spectra, which might also explain part of the chemical shift associated with —ONa groups; the —COONa changes in an extensive range making the diffraction peak broad in this space.

3.4. Functional group identification

The Gaussian peak shape function was selected to fit the FT-IR spectra, as shown in Fig. 5 and Table 6. Oxygen-containing functional groups in Zhundong coal are mainly ethoxy, hydroxy, carboxyl, and

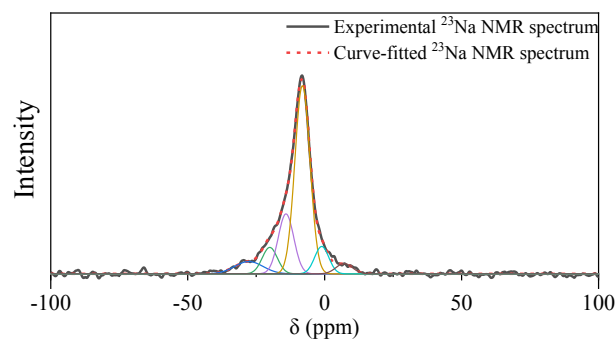


Fig. 4. ^{23}Na CP/MAS NMR spectra of Zhundong coal.

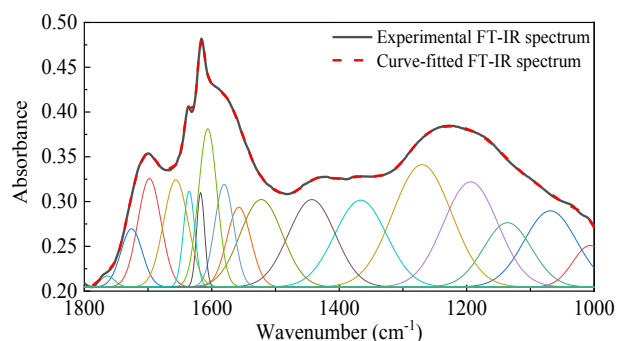


Fig. 5. FT-IR spectra of Zhundong coal.

Table 5

Assignments for peaks in ^{23}Na -CP/MAS NMR spectra.

Position/ppm	Assignment	Molar content/%
-27.6876	"-O-Na" or "-COONa"	6.86%
-20.0375	"-O-Na" or "-COONa"	7.87%
-14.1152	"-O-Na" or "-COONa"	18.39%
-8.11933	"-O-Na" or "-COONa"	55.91%
-1.07539	"-O-Na" or "-COONa"	7.63%
7.130719	NaCl	3.34%

Table 6

Curve-fitted FT-IR for Zhundong coal.

Position/ cm^{-1}	Assignment	Height	Width	Area
1006.281	OH-bend vibration of hydroxyl	0.046	63.883	3.153
1068.662	C—O	0.085	96.914	8.781
1135.890	C—O	0.072	88.605	6.769
1193.799	C—O	0.118	100.564	12.574
1269.932	C—O	0.137	108.511	15.777
1366.433	Bending vibrations of $-\text{CH}_3$ groups	0.097	95.547	9.867
1442.912	Aromatic C=C	0.098	86.471	8.984
1522.338	Aromatic C=C	0.098	77.985	8.108
1557.543	Aromatic C=C	0.089	44.296	4.203
1580.593	Aromatic C=C	0.115	35.281	4.312
1606.291	Aromatic C=C	0.177	34.264	6.446
1617.507	Aromatic C=C	0.106	14.651	1.645
1635.483	C=O	0.107	20.815	2.369
1656.343	C=O	0.120	45.433	5.787
1697.807	-COOH	0.120	42.785	5.518
1725.834	-COOH	0.065	39.532	2.736
1763.786	-COOH	0.012	27.057	0.352

carbonyl. FT-IR data related to the oxygen element provided organic oxygen in Zhundong coals as 67.7% hydroxyl (ethoxy), 15.5% carbonyl, and the remaining 16.8% distributed to carboxyl.

XPS analysis of the Zhundong coal is illustrated in Fig. 6 and Table 7. The results show that the main form of nitrogen in the coal was pyrrole nitrogen, followed by pyridine nitrogen; the sulfur in the coal was mainly thiophene and sulfone sulfur. Previous works by Ling (2015) [37] used XPS and have similar results for nitrogen and sulfur species in Zhundong samples.

4. Macromolecular modeling and verification

4.1. Macromolecular model of matrix and verification

Considering the coal model's structural diversity, we searched for various macromolecular configurations, and the calculated ^{13}C NMR and FT-IR spectrum nicely matched the experimental spectra of

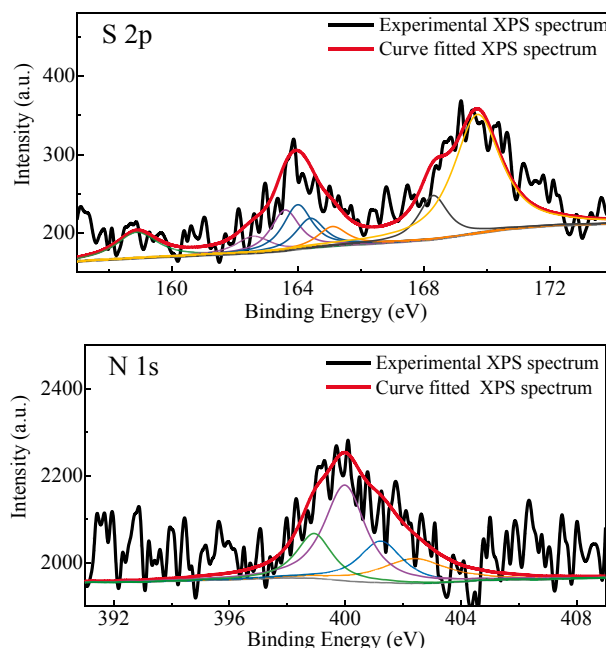


Fig. 6. Curve-fitted XPS spectra of Zhundong coal.

Table 7

Curve-fitted XPS for Zhundong coal.

Elemental	Assignment	Binding energy/eV	Molar content/%
N 1S	Oxidized nitrogen	402.40	18.37%
	Quaternary nitrogen	401.23	20.13%
	Pyrrole nitrogen	399.99	43.77%
	Pyridine nitrogen	398.93	17.73%
S 2P	Trophozoite sulfur	158.900	8.47%
	Aliphatic sulfur	162.600	4.57%
	Aromatic sulfur	163.600	9.15%
	Aromatic sulfur	164.000	10.27%
	Aromatic sulfur	164.400	6.83%
	Sulfoxide	165.100	4.53%
	Sulfone	168.300	10.27%
Inorganic sulfate	169.700	45.91%	

Zhundong coal. A detailed analysis of all of the macromolecular configurations was impractical. Here, three relatively stable three-dimensional structures of macromolecular configurations were confirmed by the absence of any imaginary frequency and were detailed in Fig. 7. (See .mol files of the proposed configurations in Supplementary Materials.) The difference in these macromolecular configurations mainly emerged in the bridging unit and the functional group's position. We summarized the bond length distribution and chemical bond breaking information obtained by the macromolecular model of Zhundong coal in Figure S4 (Supporting information), which agrees with the order of chemical bond breaking thermogravimetric experiments (detailed results are available in the Supporting Materials).

For comparison, the calculated ^{13}C NMR spectrum of Zhundong coal macromolecular and experimental spectrum of Zhundong coal are illustrated in Fig. 8. Calculated ^{13}C NMR spectra of the macromolecular model agree well with the test spectra.

The simulated FT-IR spectra of the Zhundong coal macromolecular model are qualitatively similar to the experimental FT-IR spectra of the Zhundong coal sample (Fig. 9). However, there are some differences in intensity and location due to the simulated spectra containing the intermolecular bonding information and the resonant approximation; these do not account for non-simple harmonic effects [38]. The experimental FT-IR spectra at 1110–1250 cm^{-1} have one broad peak, whereas there are several sharper peaks in the simulated FT-IR spectrum, mainly

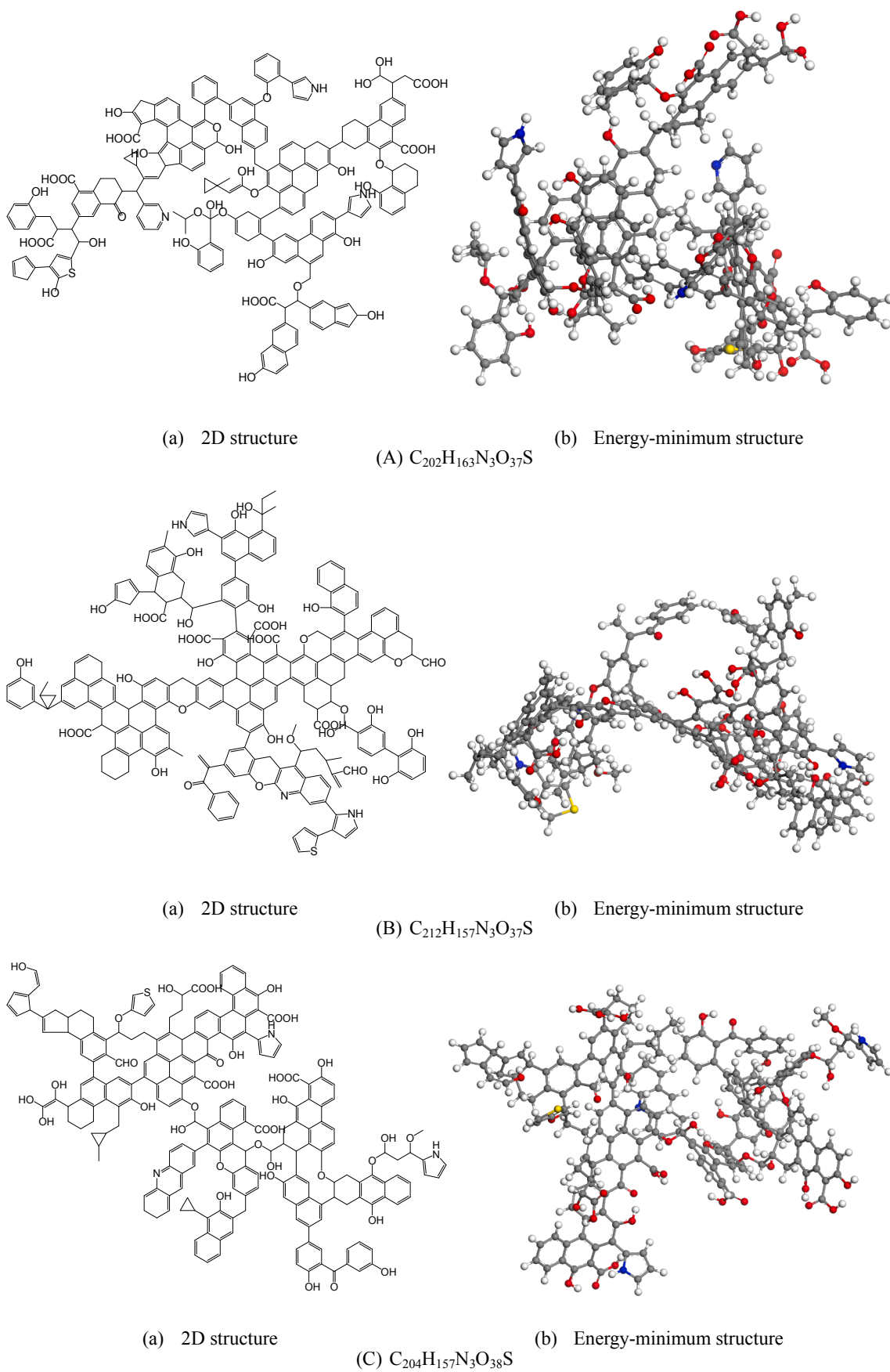


Fig. 7. Macromolecular structure model of Zhundong coal. Note: C, grey; H, white; O, red; N, blue; S, yellow. (For interpretation of the references to colour in this figure legend, the reader is referred to the web version of this article.)

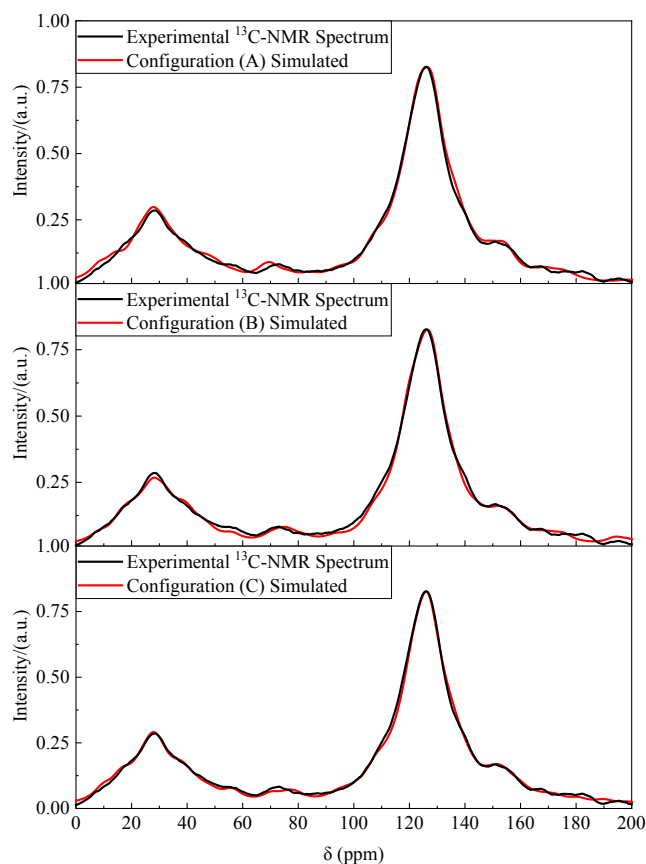


Fig. 8. Experimental ^{13}C NMR spectra of Zhundong coal compared to simulated spectra.

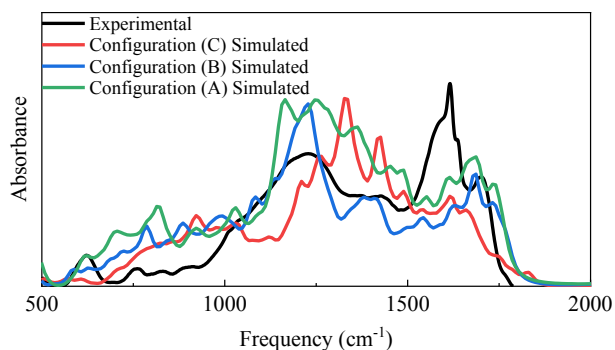


Fig. 9. Experimental infrared spectra of Zhundong coal compared to calculated spectra.

because the simulation was performed in a vacuum environment with a higher resolution. This is mainly because the simulated FT-IR spectrum of individual macromolecules of Zhundong coal were performed in a vacuum environment with a higher resolution and did not contain the intermolecular hydrogen bonding information from the experimental spectra, and this limitation is inherent to all computer molecular modeling [17].

There is good consistency between the calculated simulated ^{13}C NMR and FT-IR spectrum of the Zhundong coal macromolecular model and the Zhundong coal sample's experimental spectrum. These data collectively show that the proposed macromolecular model of Zhundong coal is a relatively creditable model for the approximate condition of statistical averages.

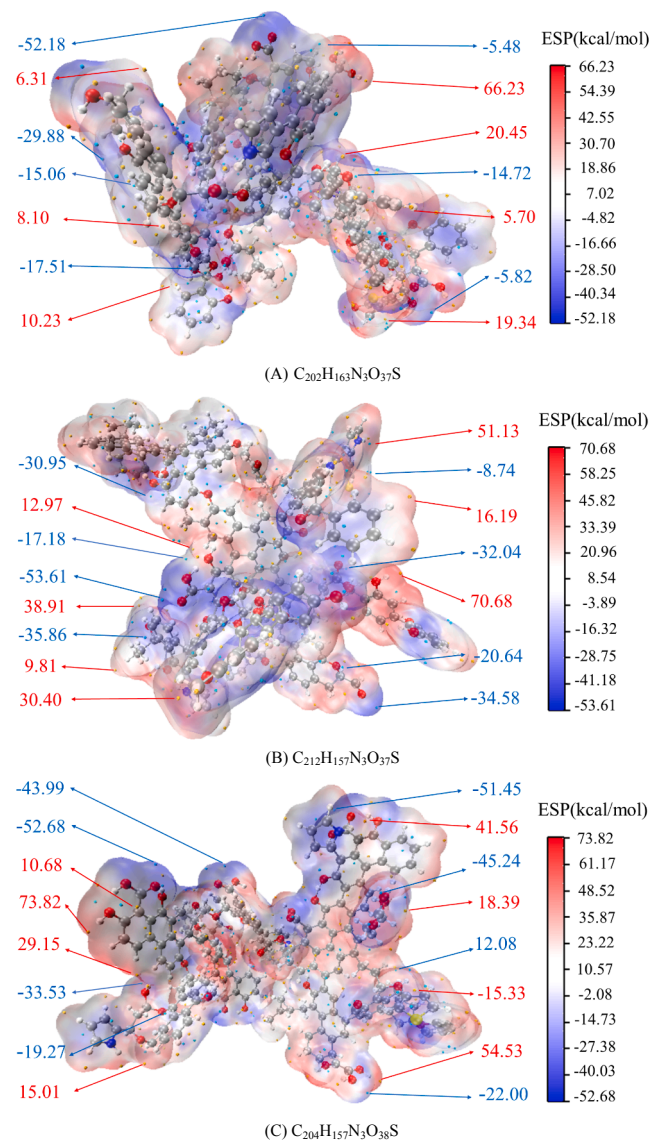


Fig. 10. Electrostatic potential (ESP) of Zhundong coal macromolecular surface. Note: maximum point, gold; minimum point, light blue. (For interpretation of the references to colour in this figure legend, the reader is referred to the web version of this article.)

4.2. Occurrence model of organic sodium and verification

The electrostatic potential (ESP) of Zhundong coal's macromolecular surface is shown in Fig. 10. The extreme points of the negative electrostatic potential are more frequently found near the oxygen atoms on carboxyl groups. The more negative electrostatic potential is, the easier cations can be drawn in. Meanwhile, there is much water in the Zhundong coal seam, rendering carboxyl functional groups on the macromolecules of Zhundong coal transform to carboxylate easily under the action of water (Carboxyl group is acidic). For the ion exchange order $\text{Na}^+ > \text{H}^+$, the sodium ion is more susceptible to capture by oxygen atoms in the carboxyl group than hydrogen ions. Therefore, considering the electrostatic and lewis acid-base interactions, the highest negative electrostatic potential area, near the carboxyl group, with (-52.18 kcal/mol, -53.61 kcal/mol, and -52.68 kcal/mol in the configuration a, b, c, respectively) were chosen as the sodium adsorption sites.

Structures of absorbed organic sodium in Zhundong coal molecular models were optimized by DFT theory (Fig. 11). Organic sodium species connect with coal molecules through the O-Na coordinated bonds

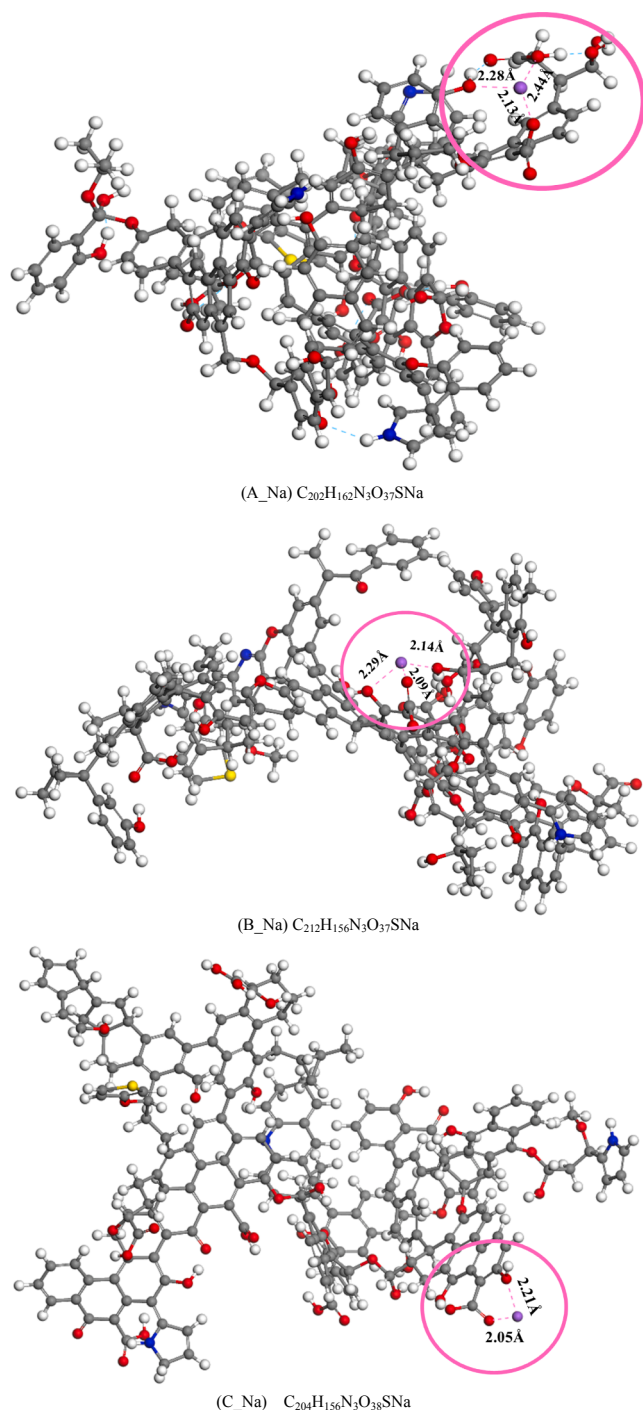


Fig. 11. DFT theory optimized structures of organic sodium-absorbed-Zhundong coal. Note: Na, purple. A_Na, B_Na, and C_Na are the corresponding structures after the adsorption of sodium in configurations A, B, and C, respectively. (For interpretation of the references to colour in this figure legend, the reader is referred to the web version of this article.)

similar to the most stable sodium acetate structure (a bidentate structure whereby both O atoms of the acetate anion coordinate with the Na atom) [39–41]. In configuration a, the nearest groups to the sodium ion are three oxygen-containing groups. Sodium is coordinated via two hydroxyls with bond lengths of 2.28 Å and 2.44 Å. These are also bonded to the carboxyl group (bond lengths 2.13 Å). In configuration b, one carboxyl and two hydroxyls are near the resulting coordination bonds to the sodium. The bond lengths are 2.09 Å, 2.29 Å, and 2.14 Å. In configuration c, the Na ion is coordinated to one carboxyl group and one

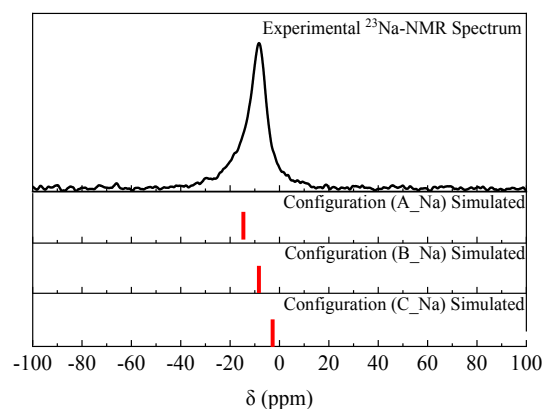


Fig. 12. ^{23}Na NMR simulated spectra of Zhundong coal.

hydroxyl (bond lengths of 2.05 Å and 2.21 Å).

In summary, sodium on the carboxyl group can form many coordinations with the oxygen-containing functional groups nearby in the macromolecular model, reflecting the Na's chemical environment's complexity (Na-O distance, Na coordination number); these findings can also be confirmed by the ^{23}Na CP/MAS NMR data in Fig. 4. The Na-O bond lengths range from 2.09 to 2.29 Å, which is consistent with a previous investigation showing that both calculated Na—O bond lengths in sodium acetate are 2.32 Å [41]. Versus the coal molecules before and after sodium adsorption, the C—C bond length near sodium becomes larger, resulting in a higher possibility of cleavage of the C—C bond. This explains the catalysis effect of sodium for gasification or combustion in the macroscopic scale in previous studies [42,43]. More detailed structural information is available in the .mol files in the [Supplementary Materials](#).

As contrast shown in Fig. 12, the calculated ^{23}Na NMR spectra of the Zhundong macromolecular model nicely reproduces the bond peak in the ^{23}Na NMR experimental spectrum of Zhundong coal, verifying the proposed model is a particularly convincing result that can elucidate the state of organic combined sodium in Zhundong coal at the approximate condition of statistical average

4.3. Occurrence model of inorganic sodium and verification

The amorphous crystal cell model of Zhundong coal was constructed using the molecular configuration of Zhundong coal constructed employing an Amorphous Cell module in the Material Studio platform. The proposed configurations of the Zhundong coal macromolecular model, as the basic unit, were put into a periodic box in a particular proportion. The ratio of unadsorbed sodium configurations to the adsorbed sodium configurations is 9:1 based on elemental and sequential extraction data. The initial amorphous cell has nine configuration A, nine configuration B, nine configuration C, one configuration A_Na, one configuration B_Na, and one configuration C_Na. The model's initial density was set to 0.1 g/m³ to avoid overlapping functional structures. To make the density reasonable, a series of molecular dynamics optimizations were performed on the initial amorphous cell model. (MD simulation details for the amorphous cell model construction are shown in section 2.6). The density of the geometry-modified amorphous cell model consists of 12,190 atoms with a molecular weight of 99,136. The molecular formula of $C_{6180}H_{4767}N_{90}O_{1120}S_{30}Na$ is 1.025 g/m³, and the edge length of the amorphous cell model is 5.438 nm.

The cause of high sodium in the Zhundong coal is related to the infiltration of highly saline (NaCl, Na₂SO₄) groundwater into the coal seam. Adsorption and cation exchange during coal formation are essential factors influencing the alkali metal occurrence. According to the sequential extraction experiment data in Table 5, the water-soluble sodium content in Zhundong coal is 0.25% after being converted to a

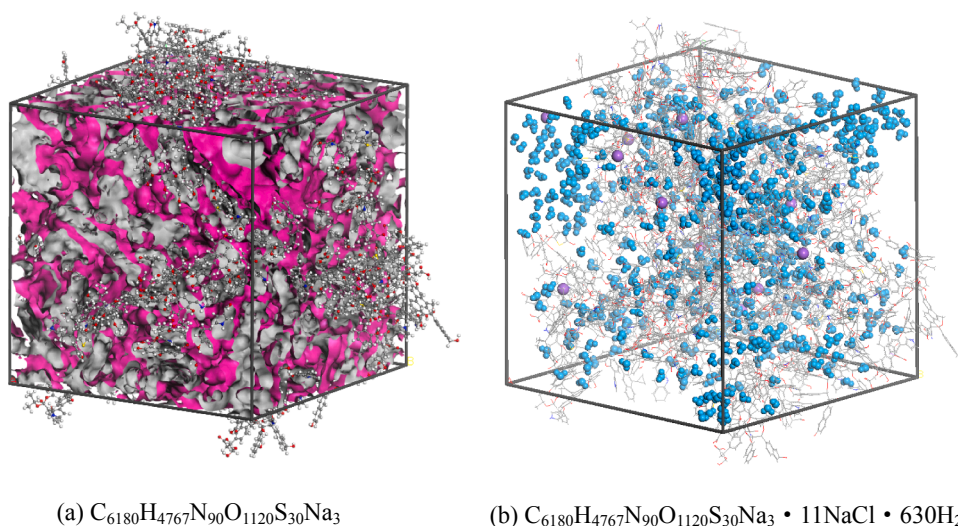


Fig. 13. The amorphous cell configurations: (a) amorphous cell without inorganic alkali metals and irregular pore within the pink area; (b) amorphous cell contains inorganic alkali metals and moisture. Note: H_2O .blue. (For interpretation of the references to colour in this figure legend, the reader is referred to the web version of this article.)

received ash-free basis. The amorphous cell of Zhundong coal should absorb 11 sodium and chloride ions. Meanwhile, to obtain wet coal models with 11.5% moisture, 630 water molecules were adsorbed to the Zhundong coal amorphous cell. The optimal adsorption location and the probability distribution of adsorption are shown in Fig. 13.

Fig. 13(a) shows that the Zhundong coal has an amorphous cell and possesses a highly disordered amorphous carbon structure with an abundance of irregular pores. This corresponds to the near-range ordered long-range disorder characteristic of the Zhundong coal structure. Probability absorption configurations of the spatial distribution of sodium ions and water molecules are shown in Fig. 13(b).

Water molecules and Na ions are mainly distributed in the three-dimensional irregular micropore, i.e., between basic units like a macromolecule. This might further explain the phenomenon whereby the extracted content of water-soluble sodium increased with increased stirring time in the sequential extraction experiments. As the stirring time increased, the sodium in the relatively larger micropore was extracted first, followed by the sodium that exists in the smaller micropore between basic molecular units. That is, more micropores become more firmly bound to the coal matrix and thus are difficult to be extracted.

The probability density distribution of H_2O and Na^+ adsorption sites in amorphous cells is illustrated in Fig. 14. The probability density distribution represents the visual statistics of adsorption sites and the magnitude of the likelihood of adsorption. Fig. 14 shows that Na^+ is preferentially placed in the same areas as moisture, as seen in the legend. This is also a good reflection of the experimental phenomenon seen in ^{23}Na CP/MAS NMR results; there is more sodium in hydrated ions than in the NaCl crystal phase.

5. Conclusions

This work investigated the occurrence forms of alkali metals in Zhundong coal via comprehensive experiments and computational chemistry (^{13}C NMR, FT-IR, XPS, and ultimate analysis experiments serve for Zhundong coal structure characters; ^{23}Na NMR and sequential extraction experiment serve for alkali occurrence characters). This then led to a macromolecular model of alkali metals in Zhundong coal at the approximate level of statistical averaging. This work is expected to provide additional evidence for actual microstructure characteristics of sodium in Zhundong coal and a practical approach for building AAEM occurrence models in the quantification and visualization in high-alkali

coal, which may be helpful for subsequent studies investigating the release mechanism of sodium during combustion and pyrolysis in view of the structure-reactive relationship. The following conclusions can be drawn from the present work.

The average molecular formula of Zhundong coal is $(C_{2080}H_{980}O_{380}N_{30}S_{10}Na)_n$. The ratio of bridge carbon to peri carbon number (X_{BP}) of Zhundong coal is 0.13. Naphthalene followed by benzene rings is the basis of the aromatic rings in the Zhundong coal macromolecular model. The FT-IR data are related to the oxygen element and provide the organic oxygen in Zhundong coal as 67.7% hydroxyl (ethoxy), 15.5% carbonyl, and the remaining 16.8% distributed to carboxyl. XPS analysis of the Zhundong coal showed that the main form of nitrogen in the coal was pyrrole nitrogen followed by pyridine nitrogen; the sulfur in the coal was mainly thiophene and sulfone sulfur. The sodium in Zhundong coal is mainly present in the water-soluble form. Combined with the ^{23}Na CP/MAS NMR and the sequential extraction experiment, we conclude that the inorganic sodium in Zhundong coal is 81.99%, 75.08% is hydrated ionic sodium, 3.34% is NaCl, and 18.01% is organic sodium; most of the water-soluble sodium is present as hydrated ionic sodium; a small part is in the NaCl crystal phase.

There is a good consistency between the calculated simulated ^{13}C CP/MAS NMR, ^{23}Na CP/MAS NMR, and the FT-IR spectrum of the macromolecular model. The proposed macromolecular model of Zhundong coal is a particularly convincing model at the approximate condition of statistical averaging. The extreme points of the surface negative electrostatic potential are more frequently found near the oxygen atoms on carboxyl groups, which may explain why sodium was most possibly absorbed into the carboxyl group. Meanwhile, sodium on the carboxyl group can form numerous coordination sites with the surrounding oxygen-containing functional groups in the macromolecular model, underscoring the complexity of the Na chemical environment (Na-O distance and Na coordination number distribute widely) as seen in the ^{23}Na CP/MAS NMR spectra. Water molecules and inorganic Na ions are mainly distributed between three-dimensional micropores between the macromolecules. Na^+ ions are preferentially absorbed in the same areas with moisture reflecting in the ^{23}Na CP/MAS NMR results.

CRediT authorship contribution statement

Cen Sun: Software, Data curation, Writing - original draft, Visualization, Investigation. **Xiaolin Wei:** Conceptualization, Supervision,

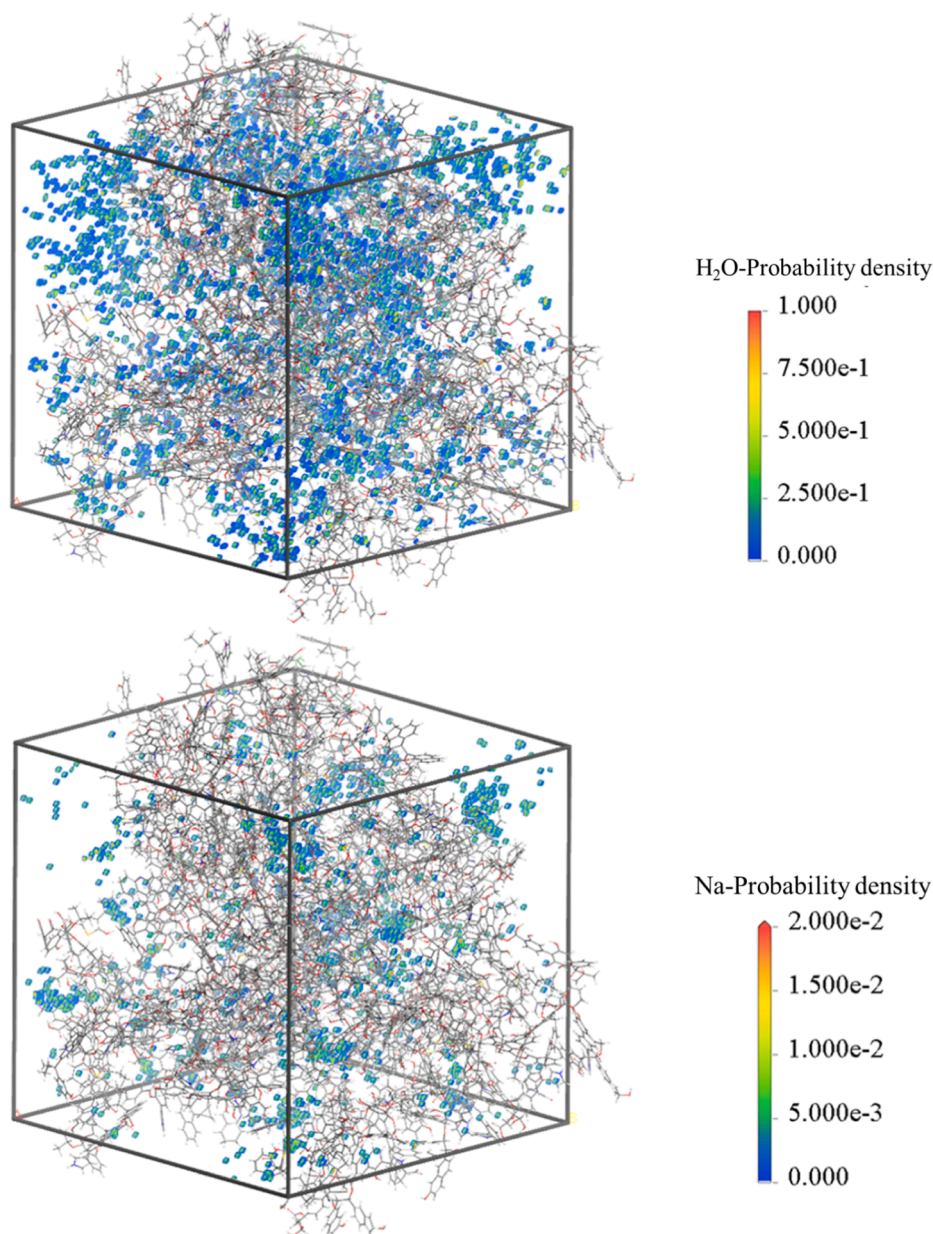


Fig. 14. The probability density distribution of H₂O and Na⁺ adsorption sites in amorphous cells.

Methodology, Funding acquisition. **Running Kang:** Writing - review & editing. **Feng Bin:** Writing - review & editing. **Sen Li:** Software, Validation.

Declaration of Competing Interest

The authors declare that they have no known competing financial interests or personal relationships that could have appeared to influence the work reported in this paper.

Acknowledgments

We gratefully acknowledge the financial support from the Natural Science Foundation of China (No. 51736010). Cen Sun thanks for the discussion with Dr. Huixin Li, Dr. Pengyun Chen, and Dr. Aixue Zhu.

Appendix A. Supplementary data

Supplementary data to this article can be found online at <https://doi.org/10.1016/j.fuel.2021.121491>.

References:

- [1] BP statistical review of world energy. <https://www.bp.com/en/global/corporate/energy-economics/statistical-review-of-world-energy.html>.
- [2] Zhou J, Zhuang X, Alastuey A, Querol X, Li J. Geochemistry and mineralogy of coal in the recently explored Zhundong large coal field in the Junggar basin, Xinjiang province, China. *Int J Coal Geol* 2010;82(1–2):51–67. <https://doi.org/10.1016/j.combustflame.2020.03.006>.
- [3] Zhu C, Qu S, Zhang J, Wang Y, Zhang Y. Distribution, occurrence and leaching dynamic behavior of sodium in Zhundong coal. *Fuel* 2017;190:189–97. <https://doi.org/10.1016/j.fuel.2016.11.031>.
- [4] Song W, Song G, Qi X, Yang S, Lu Q, Nowak W. Speciation and distribution of sodium during Zhundong coal gasification in a circulating fluidized bed. *Energy Fuel* 2017;31(2):1889–95. <https://doi.org/10.1021/acs.energyfuels.6b01610>.
- [5] Zhou Z, Shen Z, Liang Q, Liu H. Sub-particle scale study on the melting behavior of Zhundong coal ash based on the heterogeneous distribution of elements. *Combust Flame* 2020;216:223–31. <https://doi.org/10.1016/j.combustflame.2020.03.006>.

- [6] Li G, Liu Z, Li J, Fang Y, Shan J, Guo S, et al. Modeling of ash agglomerating fluidized bed gasifier using back propagation neural network based on particle swarm optimization. *Appl Therm Eng* 2018;129:1518–26. <https://doi.org/10.1016/j.applthermaleng.2017.10.134>.
- [7] Li X, Li J, Wu G, Bai Z, Li W. Clean and efficient utilization of sodium-rich Zhundong coals in China: behaviors of sodium species during thermal conversion processes. *Fuel* 2018;218:162–73. <https://doi.org/10.1016/j.fuel.2018.01.027>.
- [8] Bai X, Wang Y, Ding H, et al. Modes of occurrence of sodium in Zhundong coal. *J China Coal Soc*. 2015;40(12):2909–15. DOI:10.13225/j.cnki.jccs.2015.0204.
- [9] Yang Y, Wu Y, Zhang H, Zhang M, Liu Q, Yang H, et al. Improved sequential extraction method for determination of alkali and alkaline earth metals in Zhundong coals. *Fuel* 2016;181:951–7. <https://doi.org/10.1016/j.fuel.2016.05.014>.
- [10] Huang X, Zhang S, Jiang F, Cao Z, Zhang Y, Li H, et al. Transformation characteristics of sodium during high-sodium coal combustion process. *Energy Sources Part A* 2019;1–8. <https://doi.org/10.1080/15567036.2019.1683095>.
- [11] Wang Z, Li Q, Liu J, Huang Z, et al. Occurrence of Alkali Metals in Zhundong Coal and Its Migration During Pyrolysis Process. *Proc Chin Soc Electrical Eng*. 2014;34(S1):130–5. DOI:10.13334/j.0258-8013.pcsee.2014.s.018.
- [12] Lin X, Yang Y, Xu R, Li S, et al. Occurrence and transformation behavior of AAEMs in the flotation fraction of a typical Xinjiang coal. *J Fuel Chem Technol* 2017;45(2):157–64. <https://doi.org/10.3969/j.issn.0253-2409.2017.02.004>.
- [13] Zheng M, Li X, Guo L. Investigation of N behavior during coal pyrolysis and oxidation using ReaxFF molecular dynamics. *Fuel* 2018;233:867–76. <https://doi.org/10.1016/j.fuel.2018.06.133>.
- [14] Hao H, Chow CL, Lau D. Carbon monoxide release mechanism in cellulose combustion using reactive forcefield. *Fuel* 2020;269:117422. <https://doi.org/10.1016/j.fuel.2020.117422>.
- [15] Wang J, He Y, Li H, Yu J, Xie W, Wei H. The molecular structure of Inner Mongolia lignite utilizing XRD, solid state ¹³C NMR, HRTEM and XPS techniques. *Fuel* 2017;203:764–73. <https://doi.org/10.1016/j.fuel.2017.05.042>.
- [16] Hong D, Guo X. Molecular dynamics simulations of Zhundong coal pyrolysis using reactive force field. *Fuel* 2017;210:58–66. <https://doi.org/10.1016/j.fuel.2017.08.061>.
- [17] Meng J, Zhong R, Li S, Yin F, Nie B. Molecular model construction and study of gas adsorption of Zhaozhuang Coal. *Energy Fuel* 2018;32(9):9727–37. <https://doi.org/10.1021/acs.energyfuels.8b01940>.
- [18] Mathews JP, Chaffee AL. The molecular representations of coal – a review. *Fuel* 2012;96:1–14. <https://doi.org/10.1016/j.fuel.2011.11.025>.
- [19] Gao M, Li X, Ren C, Wang Ze, Pan Y, Guo Li. Construction of a multicomponent molecular model of fugu coal for ReaxFF-MD pyrolysis simulation. *Energy Fuel* 2019;33(4):2848–58. <https://doi.org/10.1021/acs.energyfuels.8b04434>.
- [20] Liu J, Jiang Y, Yao W, Jiang X, Jiang X. Molecular characterization of Henan anthracite coal. *Energy Fuel* 2019;33(7):6215–25. <https://doi.org/10.1021/acs.energyfuels.9b01061>.
- [21] Chen P, Gu M, Chen G, Huang X, Lin Y. The effect of metal calcium on nitrogen migration and transformation during coal pyrolysis: mass spectrometry experiments and quantum chemical calculations. *Fuel* 2020;264:116814. <https://doi.org/10.1016/j.fuel.2019.116814>.
- [22] Hong D, Cao Z, Guo X. Effect of calcium on the secondary reactions of tar from Zhundong coal pyrolysis: a molecular dynamics simulation using ReaxFF. *J Anal Appl Pyrol* 2019;137:246–52. <https://doi.org/10.1016/j.jaap.2018.11.033>.
- [23] Zhao J, Zhang Y, Wei X, Li T, Qiao Yu. Chemisorption and physisorption of fine particulate matters on the floating beads during Zhundong coal combustion. *Fuel Process Technol* 2020;200:106310. <https://doi.org/10.1016/j.fuproc.2019.106310>.
- [24] Ibarra J, Muñoz E, Moliner R. FTIR study of the evolution of coal structure during the coalification process. *Org Geochem* 1996;24(6–7):725–35. [https://doi.org/10.1016/0146-6380\(96\)00063-0](https://doi.org/10.1016/0146-6380(96)00063-0).
- [25] Hatcher PG. Chemical structural models for coalified wood (vitrinite) in low rank coal. *Org Geochem* 1990;16(4):959–68. [https://doi.org/10.1016/0146-6380\(90\)90132-J](https://doi.org/10.1016/0146-6380(90)90132-J).
- [26] Wisner WH. Conversion of Bituminous Coal to Liquids and Gases: Chemistry and Representative Processes.: Springer Netherlands, 1984. DOI:10.1007/978-94-009-6378-8_12.
- [27] Shinn JH. From coal to single-stage and two-stage products: a reactive model of coal structure. *Fuel* 1984;63(9):1187–96. [https://doi.org/10.1016/0016-2361\(84\)90422-8](https://doi.org/10.1016/0016-2361(84)90422-8).
- [28] Lei Z, Yang D, Zhang Y, Cui P. Constructions of coal and char molecular models based on the molecular simulation technology. *J Fuel Chem Technol* 2017;45(7):769–79. [https://doi.org/10.1016/S1872-5813\(17\)30038-5](https://doi.org/10.1016/S1872-5813(17)30038-5).
- [29] Yang SG, Tian JJ. Characteristics of CBM Reservoir in Eastern Part of Zhunge'er Basin. *China Coalbed Methane* 2011;8(02):20–3. <https://doi.org/10.3969/j.issn.1672-3074.2011.02.005>.
- [30] Sakanishi K, Akashi E, Nakazato T, Tao H, Kawashima H, Saito I, et al. Characterization of eluted metal components from coal during pretreatment and solvent extraction. *Fuel* 2004;83(6):739–43. <https://doi.org/10.1016/j.fuel.2003.08.022>.
- [31] Lu T, Chen F. Multiwfn: a multifunctional wavefunction analyzer. *J Comput Chem* 2012;33(5):580–92. <https://doi.org/10.1002/jcc.v33.510.1002/jcc.22885>.
- [32] Humphrey W, Dalke A, Schulten K, Schulten VMD. Visual molecular dynamics. *J Mol Graph* 1996;14(1):33–8. [https://doi.org/10.1016/0263-7855\(96\)00018-5](https://doi.org/10.1016/0263-7855(96)00018-5).
- [33] Lee C, Yang W, Parr RG. Development of the Colle-Salvetti correlation-energy formula into a functional of the electron density. *Phys Rev B Condens Matter* 1988;37(2):785–9. <https://doi.org/10.1103/physrevb.37.785>.
- [34] Becke AD. Density-functional thermochemistry. III. The role of exact exchange. *J Chem Phys* 1993;98(7):5648–52. <https://doi.org/10.1063/1.464913>.
- [35] Zhao Y, Truhlar DG. The M06 suite of density functionals for main group thermochemistry, thermochemical kinetics, noncovalent interactions, excited states, and transition elements: two new functionals and systematic testing of four M06 functionals and 12 other functionals. *Theor Chem Acc* 2008;119(5–6):525. <https://doi.org/10.1007/s00214-007-0401-8>.
- [36] Link S, Arvelakis S, Spliethoff H, De Waard P, Samoson A. Investigation of biomasses and chars obtained from pyrolysis of different biomasses with Solid-State ¹³C and ²³Na nuclear magnetic resonance spectroscopy. *Energy Fuel* 2008;22(5):3523–30. <https://doi.org/10.1021/ef800305g>.
- [37] Lin Z. The Influence Law of hydrothermal treatment on Pollutants release and migration during thermal Conversion Process of lignite. Zhejiang University. 2015. <http://d.wanfangdata.com.cn/thesis/Y2747724>.
- [38] Kesharwani MK, Brauer B, Martin MJML. Frequency and Zero-Point vibrational energy scale factors for Double-Hybrid density functionals (and other selected methods): can anharmonic force fields be avoided. *J Phys Chem A* 2014;119(9):1701–14. <https://doi.org/10.1021/jp508422u>.
- [39] Aziz EF, Ottosson N, Eisebitt S, Eberhardt W, Jagoda-Cwiklik B, Vácha R, et al. Cation-specific interactions with carboxylate in amino acid and acetate aqueous solutions: X-ray absorption and ab initio calculations. *J Phys Chem B* 2008;112(40):12567–70. <https://doi.org/10.1021/jp805177v>.
- [40] Annapureddy HVR, Dang LX. Molecular mechanism of specific ion interactions between alkali cations and acetate anion in aqueous solution: a molecular dynamics study. *J Phys Chem B* 2012;116(25):7492–8. <https://doi.org/10.1021/jp301859z>.
- [41] Zhang W-J, Hou G-L, Wang P, Xu H-G, Feng G, Xu X-L, et al. Microsolvation of sodium acetate in water: anion photoelectron spectroscopy and ab initio calculations. *J Chem Phys* 2015;143(5):054302. <https://doi.org/10.1063/1.4927668>.
- [42] Zhao Y, Xing C, Shao C, Chen G, Sun S, Chen G, et al. Impacts of intrinsic alkali and alkaline earth metals on chemical structure of low-rank coal char: semi-quantitative results based on FT-IR structure parameters. *Fuel* 2020;278:118229. <https://doi.org/10.1016/j.fuel.2020.118229>.
- [43] Gao M, Lv P, Yang Z, Bai Y, Li F, Xie K. Effects of Ca/Na compounds on coal gasification reactivity and char characteristics in H₂O/CO₂ mixtures. *Fuel* 2017;206(oct.15):107–16. <https://doi.org/10.1016/j.fuel.2017.05.079>.